JEE Journal of Ecological Engineering

Journal of Ecological Engineering, 2026, 27(3), 374–386
https://doi.org/10.12911/22998993/213874
ISSN 2299–8993, License CC-BY 4.0

Received: 2025.10.15
Accepted: 2025.11.23
Published: 2026.02.01

Deep eutectic solvent-modified hydrotalcite for carbon dioxide capture: A new generation of hybrid sorbents

Mohammed R. Abed[1], Ahmed Daham Wiheeb[1*]

[1] Chemical Engineering Department, College of Engineering, University of Diyala, Baquba, Diyala, Iraq
* Corresponding author's e-mail: chemical_grad_24_5@uodiyala.edu.iq

ABSTRACT

The critical demand for effective CO_2 capture methods is highlighted by the mitigation of greenhouse gas emissions, particularly CO_2. This is indicative of their significant influence on human well-being and global ecosystems, as well as their essential involvement in climate change. The adsorption method is a popular technique for capturing and storing CO_2. This technique demands the use of an adsorbent, one of which is hydrotalcite (HT). The impregnation of HT with deep eutectic solvents (DES) can improve its adsorption capacity. In this study, a DES composed of choline chloride (ChCl) and monoethanolamine (MEA) at a mole ratio of 1:4 was used to modify the prepared HT by the combustion-recrystallization (HTR)-impregnation (HTI) procedure employing aluminum and magnesium nitrate precursors and carbonate solutions with a 20 wt.% DES loading. Comprehensive characterization was carried out through Fourier Transform Infrared Spectroscopy (FTIR), Field Emission Scanning Electron Microscope (FESEM), and Energy-Dispersive X-ray (EDX) analysis to identify the deviations in covalent chemical bonds of molecules, surface morphology, and elemental composition of the prepared adsorbents. The FTIR results confirmed interactions between DES functional groups and the hydroxyl layers of hydrotalcite, while SEM and EDX analyses revealed surface modification and changes in elemental composition. Remarkably, the impregnated HTI with DES exhibited a good CO_2 adsorption capacity of 0.46 mmol/g at room temperature and 1 bar. Furthermore, a remarkable recyclability validates the potential of DES-impregnated hydrotalcites for advanced CO_2 capture applications.

Keywords: adsorption, carbon dioxide capture, hydrotalcite, deep eutectic solvents, choline chloride.

INTRODUCTION

The continuous rise in energy consumption, which characterizes modern lifestyles in developed nations, has adverse consequences for environmental quality and ecosystems. These negative effects are mainly driven by greenhouse gas (GHG) emissions, prompting many countries to implement stricter environmental policies. Among these gases, carbon dioxide (CO_2) is the most significant anthropogenic contributor, accounting for about 76% of emissions linked to global warming CO_2 capture is anticipated to play a crucial role in advancing the commercialization of future CCS technologies. Researchers and governments are actively exploring a variety of processes and materials for this purpose including physical and chemical absorption, adsorption, permeation via organic and inorganic membranes and cryogenic distillation (Pichura et al., 2022).

Adsorption of CO_2 is based on the ability of gases (the adsorbate) to be adsorbed on a solid surface (the adsorbent), which can then be regenerated (where CO_2 is released to reuse the adsorbent) by adjusting the system's temperature (temperature swing) or pressure (pressure swing). There are two possible methods for the adsorption to occur: First, the CO_2 molecules form new chemical covalent connections with the adsorbent surface through a process known as chemical adsorption, or chemisorption. Second, the CO_2 molecules adhering to an adsorbent surface via weak, non-covalent Van der Waals forces through a process known as physical adsorption, or physisorption (Abdullah and Shakir, 2024). Numerous investigations on different adsorbent

materials utilized in the CO_2 adsorption process have been published recently. Among these, solid adsorbents such as: activated carbon (Ahmed and Wiheeb, 2019), zeolite (Boer et al., 2023), silica (Tumurbaatar et al., 2023), metal oxide (Hakim et al., 2016) and hydrotalcite (León et al., 2010) are gaining attention as promising candidates for CO_2 capture due to their favorable properties.

Hydrotalcites (HTs) are referred to as layered double hydroxides (LDHs) in the bibliography. The LDHs consist of brucite-like layers, also known as anionic clays. The typical formula for hydrotalcites, which have been known for more than 150 years, is $[M^{2+}_{1-x} M^{3+}_{x} (OH)_2]^{x+} (A^{n-})_{x/n}. mH_2O$, where M^{2+} and M^{3+} denote divalent and trivalent cations, respectively, and A signifies the interlayered anion. The layer charge depends on the molar ratio $x = M^{3+} / (M^{3+} + M^{2+})$, which generally ranges between 0.2 and 0.4 (Bukhtiyarova, 2019). The Mg_3AlCO_3 hydrotalcite is a category of LDH usually originate in nature. HTs have fast adsorption-desorption kinetics, are competitive at temperatures between approximately 473 K and 723 K, and are positively impacted by the presence of water (Lwin and Abdullah, 2009). Furthermore, compared to other possible CO_2 adsorbents (such as calcium oxides), they exhibit superior stability throughout cycling and need less energy to regenerate. Nevertheless, a significant disadvantage of HTs for commercial application is their comparatively low CO_2 adsorption capacities. Many investigations have concentrated on altering the chemistry of HTs by swapping out their structural ions and/or adding alkali dopants in an effort to mitigate this weakness and enhance their overall adsorption performance (Sun et al., 2020). It has also been observed that using carbon-based materials such graphene oxide (GO) (Garcia et al., 2012), multi-walled nanotubes (MWCNT), and nanofibers (CNF) (Malekbala and Salari, 2020) to support HTs can improve their CO_2 performance. Despite the fact that the utilization of these carbon materials has resulted in a notable improvement in terms of intrinsic capacity and regenerability, thermal degradation of the support was noted over prolonged multicycles (Malekbala and Salari, 2020).

Deep eutectic solvents (DESs) are a class of green solvents formed by mixing a hydrogen bond donor and acceptor, resulting in a stable liquid with unique physicochemical properties such as high polarity, tunable viscosity, and strong interaction capabilities. When impregnated onto solid adsorbents, DESs can significantly modify the surface chemistry by introducing functional groups ($^-$OH, $^-$NH, or ionic species) that enhance affinity toward target molecules like CO_2. This combination improves adsorption capacity, stability, and sometimes regenerability, making DES-impregnated adsorbents a promising strategy for advancing gas separation and environmental applications. For example, silica gel impregnated with a DES achieved a CO_2 adsorption capacity of 89.32 mg/g, compared to only 15.71 mg/g for bare silica gel, representing more than a fivefold improvement (Jahanbakhshi et al., 2024). Similarly, activated carbon impregnated with a DES displayed an increase from 2.8 mmol/g (raw activated carbon) to 4.3 mmol/g after loading, due to stronger affinity between CO_2 and the introduced functional groups (Zulkurnai et al., 2018). This paper presents experimental method to prepare a novel porous DES-HT adsorbent that enhances the adsorption capacity of CO_2 from CO_2-N_2 gas mixture. Since DES is known to have high affinity for CO_2, the DES impregnated into the HT is expected to increase the capture of CO_2 by increasing its affinity adsorption as well as its good regeneration stability.

MATERIALS AND METHODS

Materials

Potassium carbonate (K_2CO_3, 98%), sodium carbonate (Na_2CO_3, 98.5%) and poly vinyl alcohol ((C_2H_4O) x, 99%) were acquired form HIMedia Laboratories Pvt. Ltd. India. Magnesium nitrate hexahydrate ($Mg(NO_3)_2 \cdot 6H_2O$, 98%) and aluminum nitrate nonahydrate ($Al(NO_3)_3 \cdot 9H_2O$, 98%) were acquired from Thomas Baker India. While, saccharose ($C_{12}H_{22}O_{11}$, 99%) were acquired from Shajanad Estate India. Monoethanolamine (MEA, 99%) were acquired from Central Drug House (P) Ltd. India. Choline Chloride (ChCl, 98%) were acquired from Loba Chemie India. Ethanol (C_2H_6O, 99.7%) from Alph Chemika India. The cylinders of N_2 gas (99.99%) and CO_2 gas (99.99%) that required to generate flue gas were acquired from the Biladi plant for gases in Iraq.

Preparation of hydrotalcite

Hydrotalcite was prepared using the combustion method as described in earlier research (Martunus et al., 2011). A total of 20 g of magnesium nitrate and 6.67 g of aluminum nitrate, with

a magnesium to aluminum mole ratio of 3, were combined in a 100 ml beaker. Subsequently, 6.67 grams of potassium carbonate were added, along with 6.67 g of a fuel source. The combination was stirred and heated to a temperature of 80 °C for a duration of 5 minutes. After that adding 2 ml of water at 90 °C while maintaining the mixture's temperature at 80 °C. The solution was stirred at a consistent speed for 10 minutes. Once the stirring period concluded, two drops of 4wt.% poly-vinyl alcohol were incorporated. Following an 8-min wait for the water to evaporate, the product transforms into a slurry and subsequently turns into a paste. The paste obtained was placed into a 50 ml crucible and then heated in a furnace at 650 °C for 5 min to yield a mixture of oxides. The obtained mixed oxides were grounded very well and after that putted into 100 ml beaker, followed by adding 50 ml of 0.1 M K_2CO_3 solution. The mixture was stirred for 5 min, then the solid was filtered and rinsed with de-ionized water before being dried at 120 °C for 20 min to yield the re-crystallized HT sample. This product was labeled as HTR. Before the metal elements were impregnated into the HTR sample, 100 g of HTR was calcined at 650 °C for 4 h in the air. The calcined solid was brought into contact with 112 ml solution contains (18.5% K_2CO_3 and 1.5% Na_2CO_3) to get 20% loading ratio. Keeping the solid and solution in contact for 1 h after that the excess liquid was removed by decantation. Drying the product at 120 °C for 16 h. The product was labeled as HTI.

Preparation of deep eutectic solvent

The DES was prepared by drying Choline chloride (ChCl) for 48 h at 65 °C to eliminate any potential moisture. Before that mono ethanol amine (MEA) was heated at 80 °C on a hot plate with stirring at 500 rpm. Subsequently, slowly adding of ChCl to MEA with a ratio of 1mole ChCl: 10 mole MEA with keeping stirring the mixture for 4 h through that the translucent color of the mixture change to the yellow to continue ridding any moisture the mixture put in the dryer at 80 °C overnight. At this point the DES now ready to use in doping HT (Nasif and Wiheeb, 2024).

Preparation of deep eutectic solvent impregnated onto the hydrotalcite

The prepared re-crystallized hydrotalcite (HTR) and impregnated hydrotalcite (HTI) were both functionalized with DES using wet impregnation method to get HTR@DES and HTI@DES. Both HTR and HTI were degassed by heating them to 200 °C for 3 h followed by cooling to 55 °C to certify the elimination of residual moisture. 10 mL of ethanol were added to the 0.6 ml of DES; the solution was gently stirred for approximately 30 min. until a homogeneous mixture was obtained. The prepared solution was added slowly and carefully to 2.35 g of HT to achieve loading of 20 wt.% DES onto the HT and the mixture was stirred for 60 min. To complete the impregnation, the mixtures will site 24 h. The residue of the mixture was dried at 100 °C for 24 h to remove any residue volatile component (Hasan et al., 2023).

CHARACTERIZATION

The chemical structure of the prepared HTR, HTI, HTI@DES and HTR@DES before and after adsorption of CO_2 as well as after desorption process were determined using Fourier transform infrared spectroscopy (FTIR), which observes deviations in covalent chemical bonds in molecules. The Shimadzu spectroscope (Shimadzu corporation FTIR Affinity-1 spectrometer, 1800, Japan) at the BPC Analysis Center/ Adhamiya/ Baghdad/ Iraq/ near Al-Nu'man Teaching Hospital. was used to acquire the FTIR spectra for the samples. The potassium bromide (KBr) pellet technique was used to record the infrared spectra within the wavenumber range of 4000-400 cm^{-1}. Before analysis, a transparent pellet was obtained by grinding the KBr and sample together in a mass ratio of 1:20 (KBr: sample) after they had been dried for 2 h at 105 °C. A uniaxial press was used to press the fine powder combination at 75 MPa, resulting in a pellet that was roughly 1 mm thin. The pellet was positioned in a sample container and exposed to the FTIR unit's infrared light perpendicularly.

The surface morphology and elemental composition were analyzed using Field Emission Scanning Electron Microscope (FESEM) from Czech, model MIRAIII (TESCAN) at the BPC Analysis Center, Adhamiya, Baghdad, Iraq. Samples were mounted on the specimen stage and vacuumed prior to analysis. The SEM is equipped with an EDX microanalysis system, with an accelerating voltage range of 200 V to 30 kV and a high-brightness Schottky emitter electron gun. The microscope provides magnification up to 1,000,000× and allows imaging under both high

vacuum and variable pressure conditions. EDX was employed to determine the elemental composition of the samples, using MnKα as the energy source, operated typically at 15 kV accelerating voltage, with an energy resolution of ~125 eV and a take-off angle of 22.4°.

Experimental procedure of CO_2 adsorption and desorption process

The experiments on CO_2 adsorption and desorption were carried out in a quartz tube fixed vertically. Four types of adsorbents (HTR, HTI, HTI@DES and HTR@DES) were employed in the CO_2 adsorption at room temperature using 15 vol% CO_2 and 85 vol% N_2 as a feed gas, signifying the amount of CO_2 contained in a power plant's flue gas. Mass flow controllers purchased from China (Beijing Ifan Peng Instrument Co., Ltd.) with a range of 0–500 ml/min were used to control the gas flow rates. In a conventional cycle, 0.5 g of adsorbent was put into a quartz tube with an inside diameter of 0.8 cm. To stop the adsorbent from escaping the quartz tube, quartz wool was used to seal both ends. The quartz tube was placed within an inside diameter of 30 cm steel tube. The heater that surrounds the stainless-steel tube is linked to a temperature controller (REX-C700, China). To reduce the physically adsorbent moisture and residual CO_2 in the adsorbent, the adsorbent was heated in a stainless-steel tube to 100 °C for 2 h at a N_2 flow rate of 40 ml/min before to the adsorption assessment. It was also allowed to cool to room temperature. Adsorption of CO_2 began at a gas flow rate of 100 ml/min with 15 vol.% CO_2 and 85 vol.% N_2. The CO_2% in the output was measured using a CO_2 gas analyzer (AtmoCheck Double from the USA) every 20 seconds until saturation was reached, which is the point at which the percentage of CO_2 in the release gas was close to that of the input gas.

Practical commercial applications depend heavily on the adsorbent's high renewability and substantial adsorption capacity in the cyclic adsorption-desorption process. In this work, the regeneration ability of the four prepared samples was evaluated with one regeneration cycle When the adsorption experiments were finished, the adsorbent was heated to 100 °C using a heater that encircles the stainless-steel tube, and the desorption studies were resumed by changing the CO_2/N_2 feed gas to N_2 gas at a flow rate of 40 ml/min. This was achieved by monitoring the CO_2 content in the discharge flow constantly until the gas analyzer showed no more CO_2. Figure 1 shows the experimental arrangement for the CO_2 adsorption-desorption process.

CO_2 analysis

The saturation level of the adsorption capacity for sorbents was determined using the integrated equation of the breakthrough curves Equation 1

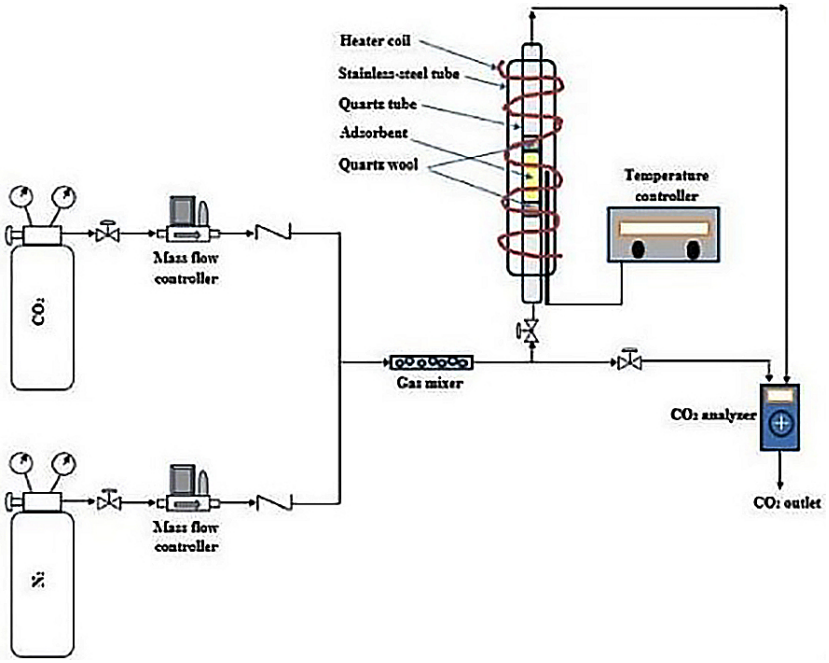

Figure 1. Configuration for the CO_2 adsorption-desorption process

and the saturation of adsorption capacity of CO_2 was plotted as a C/Co vs. time to create a breakthrough profile.

$$q = \frac{F \int_0^t (C_o - C)\, dt}{m} \quad (1)$$

where: q is the adsorption capacity of the adsorbent (mmol/gram), F represent the input volumetric flow rate of the CO_2 (ml/min), m is the mass of the adsorbent (gram), Co and C are the input and output concentrations of the CO_2 (mmol/min), t is the adsorption time (min).

The saturation adsorption capacity (q) is defined as the CO_2 adsorption capacity of C/Co =1.0, while the breakthrough adsorption capacity is defined as the CO_2 adsorption capacity of C/Co = 0.05, and the time corresponding to the breakthrough adsorption capacity is referred to as the breakthrough time (Yagub et al., 2015).

RESULTS AND DISSCUSION

Fourier transform infrared spectroscopy analysis

The FTIR spectra of the prepared HTR, HTI, HTI@DES and HTR@DES before and after CO_2 adsorption process and after regeneration are shown in Figures 2–5. All the prepared adsorbent materials (HTR, HTI, HTI@DES and HTR@DES) display IR bands assigned at 3450 cm^{-1} to 3485 cm^{-1} belong to O-H mode, existence the interlayer water molecules and hydroxyl groups in the brucite-like layers. These results give good agreement with the previously published literature (Othman et al., 2006). The observed vibrational bands at round 1640 cm^{-1} to 1660 cm^{-1} region refers to the H_2O at the interlayer water. The peak is less pronounced for the high-temperature treated sample, suggesting that water molecules are still present in the HTR, HTI, HTI@DES and HTR@DES samples' interstices to maintain the hydrotalcite structure. The bands at round 1375 cm^{-1} to 1387 cm^{-1} region correspond to the stretching vibrations of carbonate anions. The bands at around 1015 cm^{-1} to 1020 cm^{-1} and 877 cm^{-1} to 867 cm^{-1} refer to covalent carbonate. The bands at around 575 cm^{-1} to 630 cm^{-1} refer to the characteristic vibration of metal oxides (Mg-O and Al-O) (Martunus et al., 2011). The peak 3651 cm^{-1} represent the O-H stretching of structural hydroxyls (Mg-OH, Al-OH) in the layered double hydroxides (LDHs) (Frost and Erickson, 2005).

Figure 2b, shows the changes in the FT-IR spectrum of the prepared HTR after exposure to the CO_2 in the range between 1000 cm^{-1} and 1900 cm^{-1}. Exposure to CO_2 increases the intensity of the bands 1004 cm^{-1}, 1276 cm^{-1} and 1633 cm^{-1} because

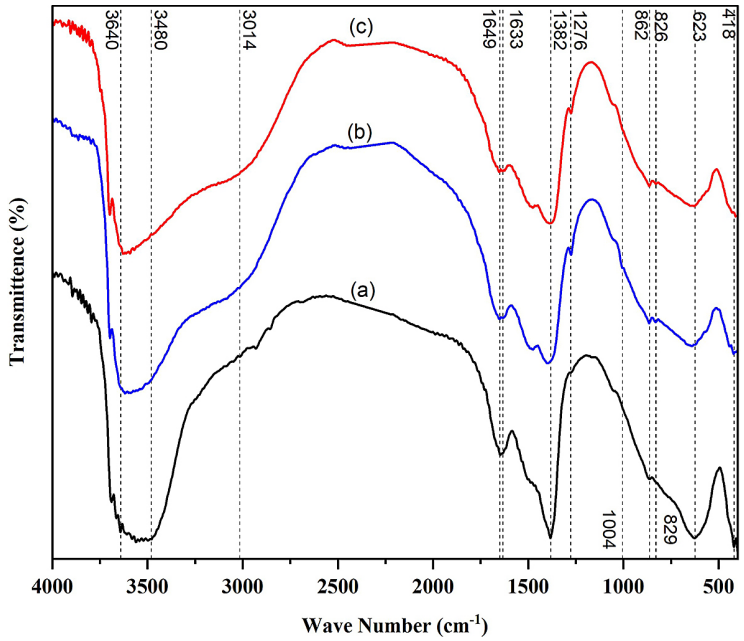

Figure 2. FTIR spectra for HTR (a) before adsorption of CO_2; (b) after adsorption of CO_2, and (c) after regeneration

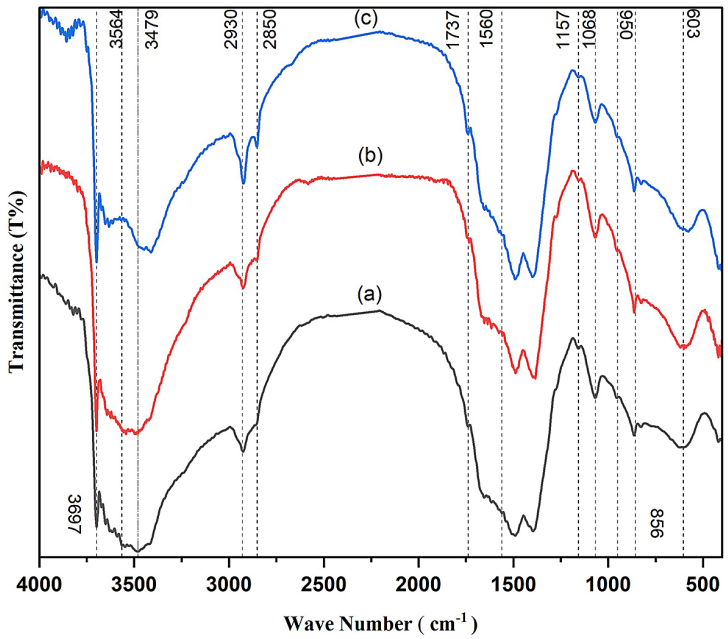

Figure 3. FTIR spectra for HTR@DES (a) before adsorption of CO_2; (b) after adsorption of CO_2, and (c) after regeneration

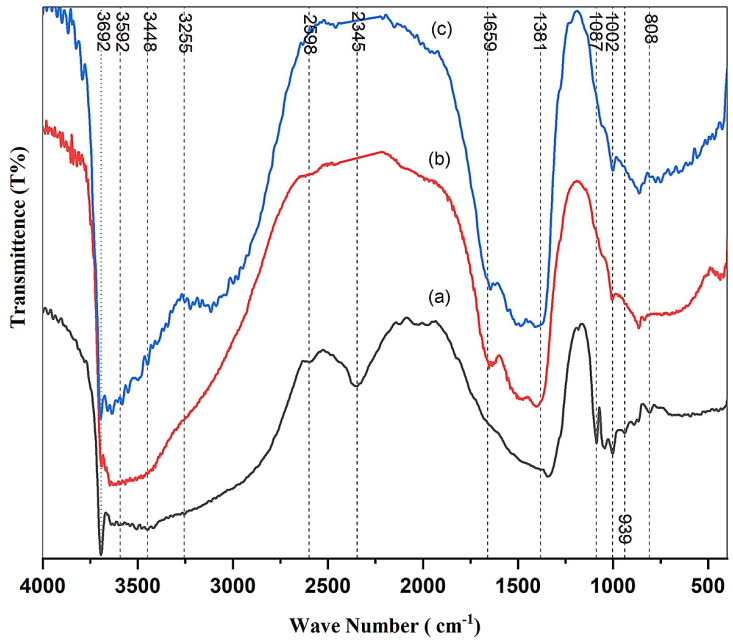

Figure 4. FTIR spectra for HTI (a) before adsorption of CO_2; (b) after adsorption of CO_2, and (c) after regeneration

of adsorption the CO_2 and forming bidentate carbonate (Coenen et al., 2017). After regeneration of the HTR sample, the FT-IR spectrum shows decrease in the intensity of the bands at around 826 cm^{-1} to 1649 cm^{-1} which mean desorbing of the CO_2 as shown in Figure 2c. On the other hand, the peak at 1004 cm^{-1} disappeared. While, the peaks at 623 cm^{-1}, 1276 cm^{-1}, and 1382 cm^{-1} kept its intensity. The intensity of the peak at 3693 cm^{-1} did not change. For the peaks kept their intensity after desorption that explain not all CO_2 adsorbed can be desorbed under these experimental conditions (Coenen et al., 2018). The FTIR spectra of the prepared HTI@DES and HTR@DES before CO_2 adsorption process is shown in Figure 3a and 4a. The peak near 950 cm^{-1} belong to the C–C symmetric in the ChCl material. The peaks at around 1068 cm^{-1} to 1083 cm^{-1} region represent the C–N

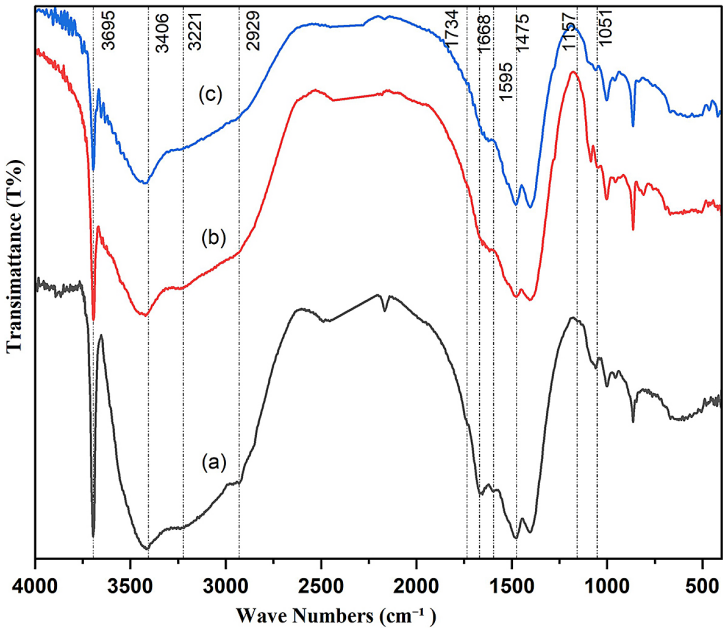

Figure 5. FTIR spectra for HTI@DES (a) before adsorption of CO_2; (b) after adsorption of CO_2, and (c) after regeneration

symmetric stretching from DES. In Figure 3a, the peak at 1157 cm^{-1} represent the C–N^+ stretching symmetry vibrations of the organic DES components (Wiheeb et al., 2015). The broadening of the ν_3 CO_3 band, together with the appearance of a shoulder at 1390 cm^{-1}, suggests the coexistence of carbonate species in different coordination environments. These include polydentate carbonate groups as well as monodentate and bidentate surface carbonates, indicating multiple bonding modes with the surface. A comparable effect is observed in the OH stretching region, where the band shift to 3475 cm^{-1} points to the presence of more weakly bonded hydroxyl groups, most likely arising from rehydration of the material (Bünger et al., 2024). The band as observed in the ~1500 cm^{-1} to 1580 cm^{-1} region was due to NH_2 bending (Wang et al., 2015).The peaks at 1739 cm^{-1} and 1651 cm^{-1} can be refer to the stretching vibration of C-O bond in the $NCOO^{-1}$ ion that formed as result of the C-N interaction because of the attending of O^- and N^- grouped attached to the ChCl:MEA compounds (Hasan et al., 2023). The peaks at around 2850 cm^{-1} to 3000 cm^{-1} region was due to stretching vibrations of the CH_2 and C–H groups. The maximum reflecting Mg–OH and Al–OH bond vibration at ~3479 cm^{-1} is broader. (Bankauskaite and Baltakys, 2014; Golestanifar and Sardarian, 2025).

The FTIR spectra of the prepared HTR@DES after CO_2 adsorption process is shown in Figure 3b. It can be observed that the intensity of the peaks at around 3651 cm^{-1} to 2850 cm^{-1} region was increased due to adsorption effects of CO_2 (Coenen et al., 2018).The peaks between 3481 cm^{-1} and 1739 cm^{-1} are important because they offer crucial details on amine impregnation and carbonate species formation (Hasan et al., 2023). CO_2 adsorption caused a change in the intensity of the peak 2850 cm^{-1}originating from the DES intensity, but not CO_2 vibrations. A small new peak between 2580 cm^{-1} to 1845 cm^{-1} is observed after adsorption indicating the presence of asymmetric O=C=O stretching in the DES impregnated in HT and which represent the CO_2 interacting with the DES (Manafpour et al., 2024). The second small peak between 2400 cm^{-1} to 2580 cm^{-1} corresponding to CO_2 gas-phase vibrational modes. The peaks at around 1630 cm^{-1} to 1660 cm^{-1} region belong to the CO_2 forming bicarbonate (HCO_3^-) by the interacting with interlayer OH of HT (Köck et al., 2013). The intensity of the small peaks at around 1650 cm^{-1} to 1550 cm^{-1} increased after exposure to the CO_2 in the adsorption process (Coenen et al., 2018). The reversible CO_2 adsorption process and the successful removal of the CO_2 are indicated by the peaks at 1274 cm^{-1} and 1573 cm^{-1} receding after regeneration.

The FTIR spectra of the prepared HTI after CO_2 adsorption process is shown in Figure 4b. It can be seen that the O–H Stretching at ~3692 cm^{-1} to 3448 cm^{-1} slight decrease and shift due to the hydroxyl interaction with the CO_2. The O-H

region at 3250–2900 cm^{-1} broadened and shifted to a lower wavenumber as a result of the CO_2 exposure to the HTI. The concurrent growth of bands at ~1620–1400 cm^{-1} and ~1060 cm^{-1} assigned to bicarbonate/carbonate confirms that the CO_2 exposure to the HTI caused the O–H region at 3250–2900 cm^{-1} to broaden and shift to a lower wavenumber, followed by stronger H-bonding and the formation of HCO_3^- species. The production of bicarbonate or carbonate species was indicated by the appearance of new peaks at approximately 1500 cm^{-1} to 1650 cm^{-1}. Interlayer Carbonate (CO_3^{2-}) stretch at ~1381 cm^{-1} to 1342 cm^{-1} shifted or disappeared, replaced by new carbonate/bicarbonate bands, indicating CO_2 uptake and intercalation (Manafpour et al., 2024). The desorption of CO_2 from HTI sample caused the peaks around 833 cm^{-1} and 1056 cm^{-1} to vanish (Coenen et al., 2018).

Figure 4c shows a small adsorption band reappearing in the 2920 cm^{-1} to 3692 cm^{-1} region, corresponding to C–H stretching of alkyl groups and O–H/N–H stretching of hydroxyl and amine functionalities. This recovery suggests that these groups, which were previously involved in CO_2 interactions, are released and revert to their initial, free or weakly hydrogen-bonded forms, which represents a partial restoration of CO_2. Strongly adsorbed carbonate and bicarbonate species that are still attached to HT or DES sites are reflected in the intensity stability in the 1650–1381 cm^{-1} range, suggesting that desorption did not occur under these circumstances. The adsorption bands at 1190 and 1002 cm^{-1} became more noticeable following desorption, suggesting that the CO_2 was eliminated under the desorption conditions.

The FTIR spectra of the prepared HTI@DES after CO_2 adsorption process is shown in Figure 5b. The sharpness of the peak at about 3695 cm^{-1} is shown to decrease following CO_2 adsorption due to the formation of HCO_3^{-2} species. The peak at around ~3560–3500 cm_{-1} are broad or weak after CO_2 adsorption because of the CO_2 interaction with OH groups. The peak at around ~3448–3200 cm^{-1} became broader due to CO_2 reaction with amine groups in DES (NH^+), leading to the formation of carbamate. The peak at 2930 cm^{-1} corresponds to C–H stretching vibrations (asymmetric CH_2 and CH_3) from the organic parts of the DES (ChCl). The peaks at around 1400–1734 cm^{-1} are the result of CO_2 adsorption, which was caused by the interaction between the HTI@DES and CO_2. The peak at 1668 cm^{-1} shifted and its intensity decreased due to the formation of bicarbonate species. The interaction between the CO_3^{-2} anion and the OH groups present in the octahedral structure of the cationic layer of HTI@DES caused the peaks at 1475, 1404, and 1595 cm^{-1} regions to lose their intensity (Mališová et al., 2018). The peaks at 1058 cm^{-1} and 1001 cm^{-1} lost their intensity and sharpness because of the CO_2 adsorption by the MEA (Wiheeb et al., 2015).

Figure 5c shows incomplete recovery of the 3695 cm^{-1} peak after regeneration indicates irreversible or strongly bound interactions between CO_2 and hydroxyl groups. Small adsorption bands that corresponded to free or weakly hydrogen-bonded hydroxyl and amine groups resurfaced in the 3675–3500 cm^{-1} range following desorption. This suggests that the removal of CO_2 partially returns these functional groups to their initial local context, demonstrating the reversible nature of weakly bound species. However, the strength of the adsorption bands at 1475, 1400, and 1085 cm^{-1} reappeared, suggesting that the carboxylate and alkyl groups in the HT/DES matrix had returned to their more homogeneous, initial states and that weakly interacting CO_2 species had been eliminated.

Surface morphology and elemental composition analysis

The SEM images of the prepared HTR, HTI, HTI@DES and HTR@DES adsorbents are shown in Figure 6. It can be observed form Figure 6a that the agglomeration of micro-particles of HTR less order with sharp edges distributed on the surface. Morphology clearly revealed an irregular-shaped surface, where fragmented and ruptured surface texture pores due to the amorphous structure. Nevertheless, the SEM image in Figure 6b for HTR@DES sample exhibited remarkable changes on the surface morphology due to the addition of DES to HTR. Typically, HT exhibits a lamellar structure with irregularly shaped surfaces and fragmented pores due to its amorphous nature. However, upon DES treatment, SEM images reveal a transformation into a more ordered and porous structure, indicating enhanced crystallinity. This morphological change suggests that DES not only aids in recrystallization but also improves the material's properties for adsorption. Figure 6c and 6d shows the SEM images of the HTI and HTI@DES samples. It can be observed that both the HTI and HTI@DES

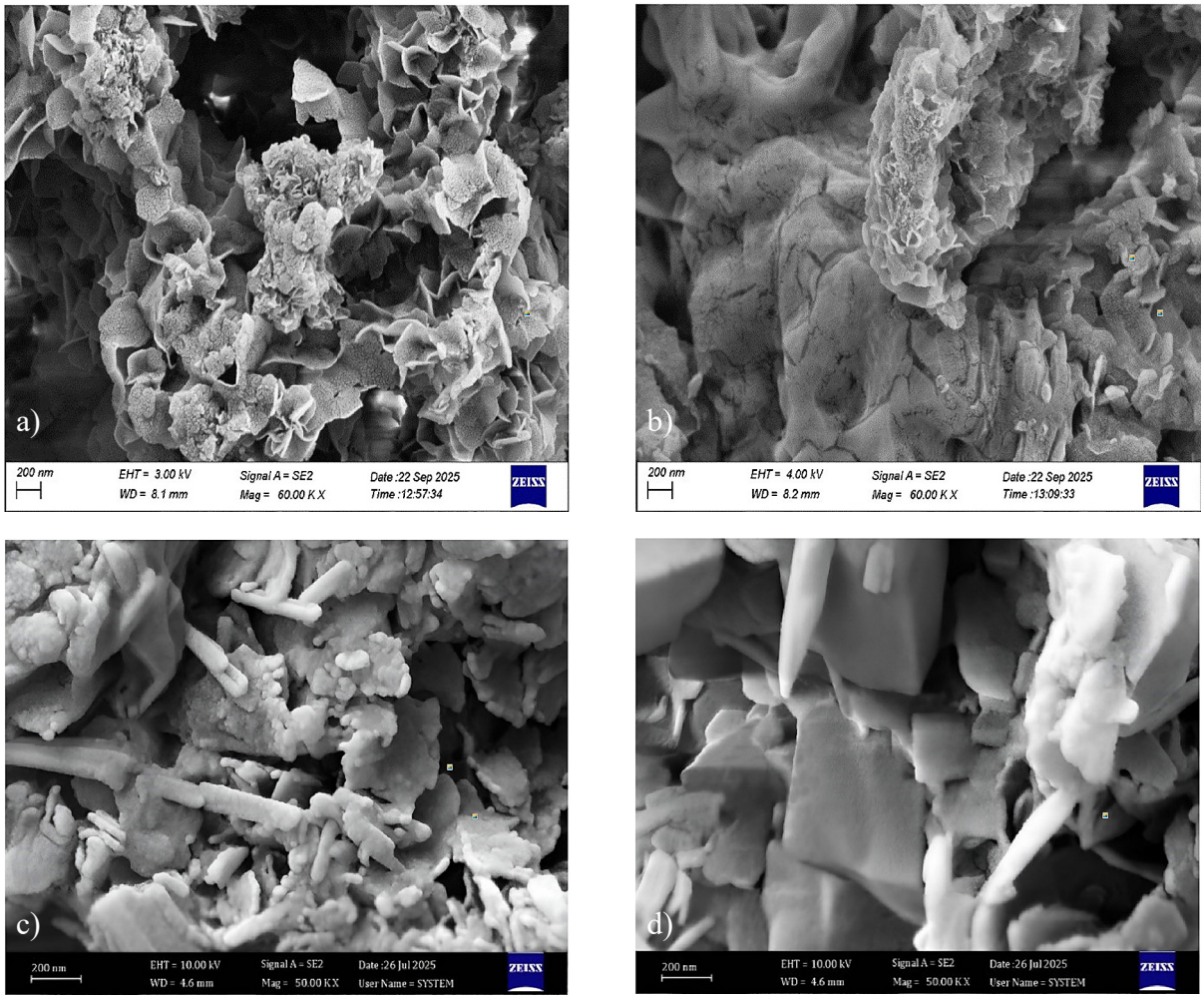

Figure 6. SEM Images of (a) HTR; (b) HTR@DES; (c) HTI; and (d) HTI@DES

samples exhibit ordered macro particle agglomeration; however, the HTI@DES sample exhibits greater order and crystallinity. The particles may be loosely stacked or somewhat aggregated for the HTI. The DES can fill micro-pores or adhere to surfaces, reducing visible roughness. Depending on the DES interaction and the texture of the HTI@DES, the platelet structure may appear more coated or smoother. The addition of DES alters porosity, possibly reducing the observed surface area by partially blocking some pores with DES molecules. As a result of DES's ability to function as a binder, platelets may appear more compacted or aggregated. The edges of the HTI are harsh, jagged, and uneven in Figure 6c, whereas the edges of the HTI@DES are more uniform, smooth, and nearly rounded in Figure 6d (Erickson et al., 2005, Bhavani et al., 2021, Sahu et al., 2012).

The energy binding of the HTR, HTI, HTI@DES, and HTR@DES samples is displayed in Figure 7. Every sample was calcined at 650 °C. Despite its little quantity, the elemental potassium has the strongest energy binding in the hydrotalcite network. Whether or not the samples were treated with the carbonate solution or DES, the energy for each element stayed constant. The elemental composition of the particles present on the material surface was analyzed using EDX. Table 1 summarizes the elemental analysis results for the HTR, HTI, HTI@DES, and HTR@DES samples together with their Mg/Al molar ratios. The HTI@DES sample exhibits a higher Mg/Al atomic ratio (~3.95) compared to the pristine HTI (~2.56). The atomic ratio of Mg/Al for HTR@DES sample (~4.77) was very near from the atomic ratio of Mg/Al for HTR sample (~4.94). This rise implies that the elemental composition may have been affected by DES impregnation, possibly by changing the distribution of Mg and Al in the hydrotalcite structure. These modifications affect the material's structural characteristics (Lian et al., 2022, Coenen et al., 2018). The observed increase in the Mg/Al ratio may

partially result from a reduction in the measured Al content due to the lower sample mass. Nevertheless, the concentrations of all metal elements, including carbon, were observed decreased after impregnation with deep eutectic solvent Figure 7 a, 7b, 7c and 7d which may be attributed to the removal of loosely bound species during the impregnation steps (Jaramillo et al., 2016).

CO_2 adsorption behavior

The adsorbent was experimentally investigated at room temperature and with a gas flow rate of 100 ml/min containing 15 vol.% CO_2 and 85 vol.% N_2 in order to comprehend the adsorption behavior of CO_2 onto 0.5 g of HTR, HTR@DES,

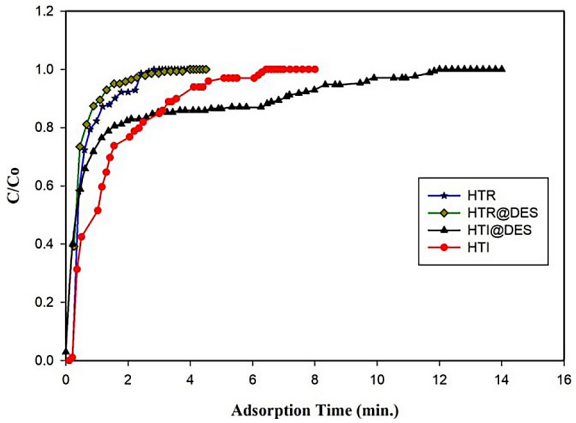

Figure 8. Breakthrough profile of CO_2 adsorption via (a) HTR; (b) HTR@DES; (c) HTI; and (d) HTI@DES

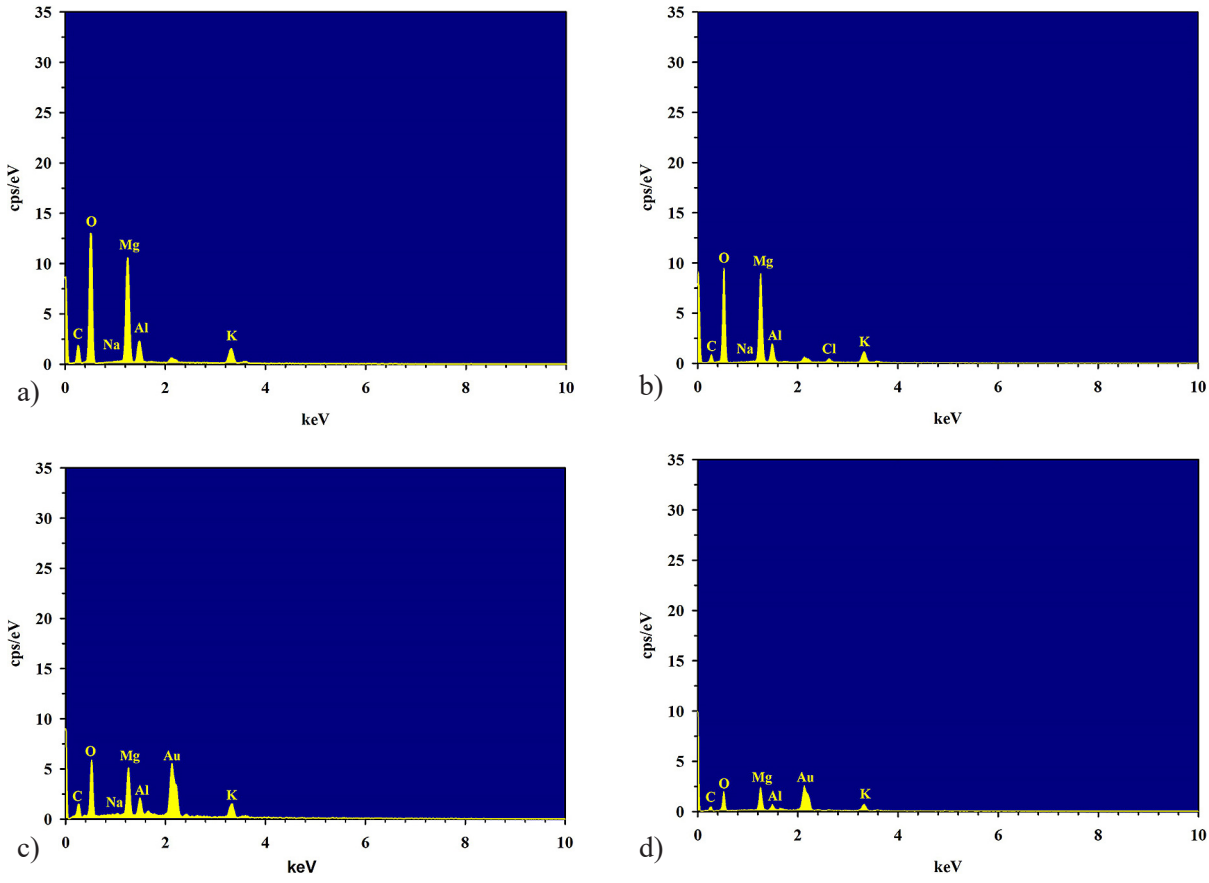

Figure 7. EDX analysis of (a) HTR; (b) HTR@DES; (c) HTI; and (d) HTI@DES

Table 1. Chemical composition of adsorbent samples from EDX analysis

Adsorbent	Mg/Al in analysis	Chemical composition, wt.%					
		Mg	Al	O	C	K	Na
HTR	~4.94	15.04	3.38	56.84	20.62	4.12	0
HTR@DES	~4.77	16.71	3.89	55.48	14.05	4.08	0
HTI	~ 2.56	21.9	9.5	33.8	6.9	27.4	0.6
HTI@DES	~ 3.95	26	7.3	29.3	5.2	32.2	0

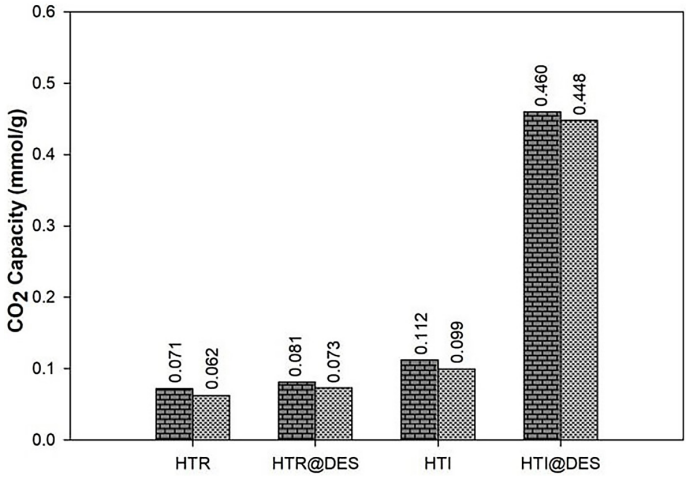

Figure 9. CO_2 adsorption capacity of two cycles for HTR; HTR@DES; HTI; and HTI@DES

HTI, and HTI@DES. The CO_2 breakthrough curve for adsorbents is plotted against adsorption time in Figure 8. It can be observed that the C/Co increases with time until it reaches 1.0, which denotes the adsorbent reaching saturation. The general form of the breakthrough curves for CO_2 adsorption onto HTR, HTR@DES, HTI, and HTI@DES was as anticipated; it resembled breakthrough curves for other HT adsorbents that have been documented in the literature (Ficicilar and Dogu, 2006). As inferred from the experimental breakthrough curve in Figure 8, the saturation time for CO_2 adsorption on HTI was significantly longer than HTR. This may have resulted from the HTI being impregnated with 18.5% K_2CO_3 and 1.5% Na_2CO_3 (Martunus et al., 2011). On the other hand, longer breakthrough times were observed when using HTR@DES and HTI@DES as adsorbents. This may be explained by the interaction of the DES functional groups (–OH, –NH, Choline and Cl^-) with the hydroxyl layers of HT, which stabilizes and modifies the surface, as demonstrated in the FTIR results, where the presence of DES functional groups on HT is indicated by new peaks. These new functional groups-hydroxyl and amine groups-create a novel CO_2 adsorption site. Figure 9 shows the adsorption capacities for 0.5 g of HTR, HTR@DES, HTI, and HTI@DES adsorbents at room temperature for two cycles. It is observed that HTI@DES exhibited highest adsorption capacity of CO_2 followed by HTI, HTR@DES and HTR. The highest CO_2 adsorption capacity of HTI@DES was 0.46 mmol CO_2/g of the adsorbent. While, the CO_2 adsorption capacity of the HTR decreased to reach 0.072 mmol CO_2/g adsorbent. The adsorption capacity of CO_2 at the first adsorption cycle was almost nearly identical to the second cycle. The addition of K_2CO_3, Na_2CO_3, and DES to hydrotalcite greatly increases the adsorption capacity of CO_2. This is compatible with hydrotalcite that has been prepared in the literature, including HT-TDD (Hydrotalcite-Tetradecanedioate) (0.369 mmol/g) and modified HT with the Tetradecanedioate-calcined (TDD–C) (0.065 mmol CO_2/g sorbent) (Cantador-Fernández et al., 2021).

CONCLUSIONS

Recrystallized and impregnated hydrotalcite was successfully prepared by the combustion process using the source as fuel at a calcination temperature of 650 °C. Hydrotalcite has been effectively impregnated with 20 wt.% of the prepared deep eutectic solvent, which is made up of ChCl and MEA at a mole ratio of 1:4. FTIR analysis confirmed the presence of characteristic hydroxyl and carbonate groups, as well as interactions between DES functional groups and the HT layers, indicating successful impregnation. SEM images revealed that DES treatment induced morphological changes and increasing surface smoothness, which enhanced CO_2 adsorption capacity. The CO_2 adsorption capacity of the recrystallized hydrotalcite increased from 0.071 mmol/g to 0.0811 mmol/g after impregnation with DES, whereas the adsorption capacity of CO_2 of the impregnated hydrotalcite increased from 0.112 mmol/g to 0.46 mmol/g after impregnation with DES. Overall, the hydrotalcite impregnated with DES improved structural and surface properties, demonstrating its potential as a more efficient

adsorbent for applications such as CO_2 capture. The comprehensive enhanced structural and surface characteristics of the DES-modified impregnated hydrotalcite indicated potential as a more potent adsorbent for CO_2 capture.

Acknowledgement

The authors gratefully acknowledge the Chemical Engineering Department/ College of Engineering/ University of Diyala for supporting this research.

REFERENCES

1. Abdullah, N. T., Shakir, I. K. (2024). Efficient carbon dioxide capture in packed columns by solvents blend promoted by chemical additives. *Journal of Ecological Engineering, 25*(10), 1–15. https://doi.org/10.12911/22998993/191436
2. Ahmed, R. E., Wiheeb, A. D. (2019). Enhancement of carbon dioxide absorption into aqueous potassium carbonate by adding amino acid salts. *Materials Today: Proceedings, 20*(17), 401–406. https://doi.org/10.1016/j.matpr.2019.09.198
3. Bankauskaite, A., Baltakys, K. (2014). The formation of different Mg–Al LDHs (Mg/Al = 2:1) under hydrothermal conditions and their application for Zn^{2+} ions removal. *Science of Sintering, 46*(1), 95–106. https://doi.org/10.2298/SOS1401095B
4. Bhavani, A. G., Wani, T., Maaruf, A., Prasad, T. (2021). Effect of ageing process on crystal morphology of Co-Mg-Al hydrotalcite. *Materials Today: Proceedings, 44*(2), 1827–1833. https://doi.org/10.1016/j.matpr.2020.12.390
5. Boer, D. G., Langerak, J., Pescarmona, P. P. (2023). Zeolites as selective adsorbents for CO_2 separation. *ACS Applied Energy Materials, 6*(5), 2634–2656. https://doi.org/10.1021/acsaem.2c03605
6. Bukhtiyarova, M. V. (2019). A review on effect of synthesis conditions on the formation of layered double hydroxides. *Journal of Solid State Chemistry, 269*, 494–506. https://doi.org/10.1016/j.jssc.2018.10.018
7. Bünger, L., Garbev, K., Ullrich, A., Stemmermann, P., Stapf, D. (2024). Mixed-matrix organo-silica–hydrotalcite membrane for CO_2 separation part 1: Synthesis and analytical description. *Membranes, 14*(8), 170. https://doi.org/10.3390/membranes14080170
8. Fernandez, D. C., Morales, D. S., Jiménez, J. R., Fernández-Rodríguez, J. M. (2021). *CO_2 adsorption by organohydrotalcites at low temperatures and high pressure. Chemical Engineering Journal, 431*, 134324. https://doi.org/10.1016/j.cej.2021.134324.
9. Coenen, K. T., Gallucci, F., Mezari, B., Hensen, E. J. M., van Sint Annaland, M. (2018). An in-situ IR study on the adsorption of CO_2 and H_2O on hydrotalcites. *Journal of CO_2 Utilization, 24*, 228–239. https://doi.org/10.1016/j.jcou.2018.01.008
10. Coenen, K. T., Gallucci, F., Pio, G., Cobden, P. D., van Dijk, E., Hensen, E. J. M., van Sint Annaland, M. (2017). On the influence of steam on the CO_2 chemisorption capacity of a hydrotalcite-based adsorbent for SEWGS applications. *Chemical Engineering Journal, 314*, 554–569. https://doi.org/10.1016/j.cej.2016.12.013
11. Coenen, K., Gallucci, F., Hensen, E., van Sint Annaland, M. (2018). CO_2 and H_2O chemisorption mechanism on different potassium-promoted sorbents for SEWGS processes. *Journal of CO_2 Utilization, 25*, 180–193. https://doi.org/10.1016/j.jcou.2018.04.002
12. Erickson, K. L., Bostrom, T. E., Frost, R. L. (2005). A study of structural memory effects in synthetic hydrotalcites using environmental SEM. *Materials Letters, 59*(2–3), 773–777. https://doi.org/10.1016/j.matlet.2004.08.035
13. Ficicilar, B., Dogu, T. (2006). Breakthrough analysis for CO_2 removal by activated hydrotalcite and soda ash. *Catalysis Today, 115*(1–4), 258–264. https://doi.org/10.1016/j.cattod.2006.02.058
14. Frost, R. L., Erickson, K. L. (2005). Raman spectroscopic study of the hydrotalcite desautelsite $Mg_6Mn_2CO_3(OH)_{16}\cdot 4H_2O$. *Spectrochimica Acta Part A: Molecular and Biomolecular Spectroscopy, 61*(11–12), 2697–2701. https://doi.org/10.1016/j.saa.2004.10.012
15. Garcia-Gallastegui, A., Iruretagoyena, D., Gouvea, V., Mokhtar, M., Asiri, A. M., Basahel, S. N., Al-Thabaiti, S. A., Alyoubi, A. O., Chadwick, D., Shaffer, M. S. P. (2012). Graphene oxide as support for layered double hydroxides: Enhancing the CO_2 adsorption capacity. *Chemistry of Materials, 24*, 4531–4539. https://doi.org/10.1021/cm3018264
16. Golestanifar, L., Sardarian, A. R. (2025). Introduction and characterization of a novel Cu(II)-based quaternary deep eutectic solvent and its application in the efficient synthesis of triazoles and tetrazoles. *RSC Advances, 15*, 3389–3405. https://doi.org/10.1039/D4RA08090D
17. Hakim, A., Marliza, T. S., Abu Tahari, N. M., Wan Isahak, R. W. N., Yusop, R. M., Mohamed Hisham, W. M., Yarmo, A. M. (2016). Studies on CO_2 adsorption and desorption properties from various types of iron oxides (FeO, Fe_2O_3, and Fe_3O_4). *Industrial & Engineering Chemistry Research, 55*(29), 7888–7897. https://doi.org/10.1021/acs.iecr.5b04091
18. Hasan, H. F., Al-Sudani, F. T., Albayati, T. M., Salih, I. K., Harharah, H. N., Majdi, H. S., Saady, N. M. C., Zendehboudi, S., Amari, A. (2023). Synthesizing and characterizing a mesoporous silica adsorbent

for post-combustion CO_2 capture in a fixed-bed system. *Catalysts, 13*(9), 1267. https://doi.org/10.3390/catal13091267

19. Jahanbakhshi, M., Ghaemi, A., Helmi, M. (2024). Impregnation of silica gel with choline chloride-MEA as an eco-friendly adsorbent for CO_2 capture. *Scientific Reports, 14*, 15208. https://doi.org/10.1038/s41598-024-66334-0
20. Jaramillo, L. Y., Posada-Correa, J. C., Pabón-Gelves, E., Ramos-Ramírez, E., Gutiérrez-Ortega, N. L. (2016). Thermal and mechanical properties of nanocomposites based on polyethylene and Mg/Al hydrotalcite. *MRS Online Proceedings Library, 1817*, 48. https://doi.org/10.1557/opl.2016.48
21. Köck, E.-M., Kogler, M., Bielz, T., Klötzer, B., Penner, S. (2013). *In situ* FT-IR spectroscopic study of CO_2 and CO adsorption on Y_2O_3, ZrO_2, and yttria-stabilized ZrO_2. *The Journal of Physical Chemistry C, 117*(34), 17666–17673. https://doi.org/10.1021/jp405625x
22. León, M., Díaz, E., Bennici, S., Vega, A., Ordóñez, S., Auroux, A. (2010). Adsorption of CO_2 on hydrotalcite-derived mixed oxides: Sorption mechanisms and consequences for adsorption irreversibility. *Industrial & Engineering Chemistry Research, 49*(8), 3663–3671. https://doi.org/10.1021/ie902072a
23. Lian, Z. Y., Zhang, Y., Wang, X. Z. (2022). Manufacturing of high quality hydrotalcite by computational fluid dynamics simulation of an impinging jet crystallizer. *Ceramics International, 48*(11), 14935–14942. https://doi.org/10.1016/j.ceramint.2022.02.081
24. Lwin, Y., Abdullah, F. (2009). High temperature adsorption of carbon dioxide on Cu–Al hydrotalcite-derived mixed oxides: Kinetics and equilibria by thermogravimetry. *Journal of Thermal Analysis and Calorimetry, 97*(3), 885–889. https://doi.org/10.1007/s10973-009-0156-7
25. Mališová, M., Horňáček, M., Mikulec, J., Hudec, P., Jorík, V. (2018). FTIR study of hydrotalcite. *Acta Chimica Slovaca, 11*, 147–156. https://doi.org/10.2478/acs-2018-0021
26. Malekbala, M. R., Soltani, S., Abdul Rashid, S., Chuah Abdullah, L., Rashid, U., Nehdi, I. A., Choong, T. S. Y., Teo, S. H. (2020). Optimization of the process of chemically modified carbon nanofibers for CO_2 capture. *Materials, 13*(7), 1775. https://doi.org/10.3390/ma13071775
27. Manafpour, A., Feyzi, F., Rezaee, M. (2024). An environmentally friendly deep eutectic solvent for CO_2 capture. *Scientific Reports, 14*, Article 19744. https://doi.org/10.1038/s41598-024-70761-4
28. Martunus, M. R., Othman, W. J. N., Fernando, W. J. N. (2011). Elevated temperature carbon dioxide capture via reinforced metal hydrotalcite. *Microporous and Mesoporous Materials, 138*(1–3), 29–36. https://doi.org/10.1016/j.micromeso.2010.09.023
29. Nasif, H. K., Wiheeb, A. D. (2024). Absorption-desorption characteristics of the synthesized deep eutectic solvents for carbon dioxide capture. *Diyala Journal of Engineering Sciences, 17*(3), 115–129. https://doi.org/10.24237/djes.2024.17308.
30. Othman, M., Anuar, M. R., Fernando, W. J. N. (2012). Production of layered hydrotalcite using tapai as fuel. *Advanced Materials Research, 545*, 401–404. https://doi.org/10.4028/www.scientific.net/AMR.545.401
31. Pichura, V., Potravka, L., Vdovenko, N., Biloshkurenko, O., Stratichuk, N., Baysha, K. (2022). Changes in climate and bioclimatic potential in the Steppe zone of Ukraine. *Journal of Ecological Engineering, 23*(12), 189–202. https://doi.org/10.12911/22998993/154844
32. Sahu, P. K., Jasra, R. V., Parikh, P. A. (2012). Hydrotalcite: Recyclable, novel heterogeneous catalyst for the synthesis of 2,3-dihydro-2-thioxopyrimidin-4(1H)-ones. *Catalysis Science & Technology, 2*(4), 760–765.
33. Sun, L., Yang, Y., Wang, W., Gao, L., Shen, B. (2020). Enhancement of CO_2 adsorption performance on hydrotalcites impregnated with alkali metal nitrate salts and carbonate salts. *Industrial & Engineering Chemistry Research, 59*(13), 6043–6052. https://doi.org/10.1021/acs.iecr.9b05700
34. Tumurbaatar, O., Popova, M., Mitova, V., Shestakova, P., Koseva, N. (2023). Engineering of silica mesoporous materials for CO_2 adsorption. *Materials, 16*(11), 4179. https://doi.org/10.3390/ma16114179
35. Wang, X., Chen, L., Guo, Q. (2015). Development of hybrid amine-functionalized MCM-41 sorbents for CO_2 capture. *Chemical Engineering Journal, 260*, 573–581. https://doi.org/10.1016/j.cej.2014.08.107
36. Wiheeb, A. D., Ahmad, M. A., Murat, M. N., Kim, J., Othman, M. R. (2015). Surface affinity and interdiffusivity of carbon dioxide inside hydrotalcite–silica micropores: CO_2 interdiffusion inside HT–Si micropores. *Journal of Porous Media, 18*(4), 379–388. https://doi.org/10.1615/JPorMedia.v18.i4.20
37. Yagub, M. T., Sen, T. K., Afroze, S., Ang, H. M. (2015). Fixed-bed dynamic column adsorption study of methylene blue onto pine cone. *Desalination and Water Treatment, 55*(5), 1026–1039. https://doi.org/10.1080/19443994.2014.924034
38. Zulkurnai, N. Z., Md Ali, U. F., Ibrahim, N., Manan, N. S. A. (2018). Carbon dioxide capture by deep eutectic solvent impregnated sea mango activated carbon. *E3S Web of Conferences, 34*, 02030. https://doi.org/10.1051/e3sconf/20183402030